# Discontinuity induced bifurcations in a model of Saccharomyces cerevisiae

D.J.W. Simpson [a,*], D.S. Kompala [b], J.D. Meiss [a,1]

[a] Department of Applied Mathematics, University of Colorado, Boulder, CO 80309-0526, USA

may be extremely complicated, see for instance [20,12,14] and references within.

A piecewise-smooth, continuous system is one that is everywhere continuous but non-differentiable on switching manifolds. In such a system, the collision of a mathematical equilibrium (i.e., steady state, abbreviated to equilibrium throughout this paper) with a switching manifold may give rise to a discontinuous bifurcation. As the equilibrium crosses the switching manifold, its associated eigenvalues generically change discontinuously. This may produce a stability change and bifurcation. In two-dimensional systems, all codimension-one discontinuous bifurcations have been classified [22], but in higher dimensions there are more allowable geometries and no general classification is known. See for instance [23,24] for recent investigations into three-dimensional systems.

In this paper we present an analysis of discontinuity induced bifurcations in the eight-dimensional S. cerevisiae model of Jones and Kompala [9]. The model equations are stated in Section 2. In Section 3 we illustrate a two-parameter bifurcation set indicating parameter values at which stable oscillations occur. The bifurcation set also shows curves corresponding to codimension-one discontinuous bifurcations. These bifurcations are analogous to saddle-node and Andronov–Hopf bifurcations in smooth systems. Bifurcations relating to stable oscillations are described in Section 4. We observe period-adding sequences over small regions in parameter space. In Section 5 we provide rigorous unfoldings of codimension-two scenarios seen in the bifurcation set from a general viewpoint. Finally Section 6 presents conclusions.

## 2. A model of the growth of *S. cerevisiae*

Jones and Kompala [9] give the following model equations:

$$\frac{dX}{dt} = \left(\sum_i r_i \nu_i - D\right) X,$$

$$\frac{dG}{dt} = \left(\right.$$

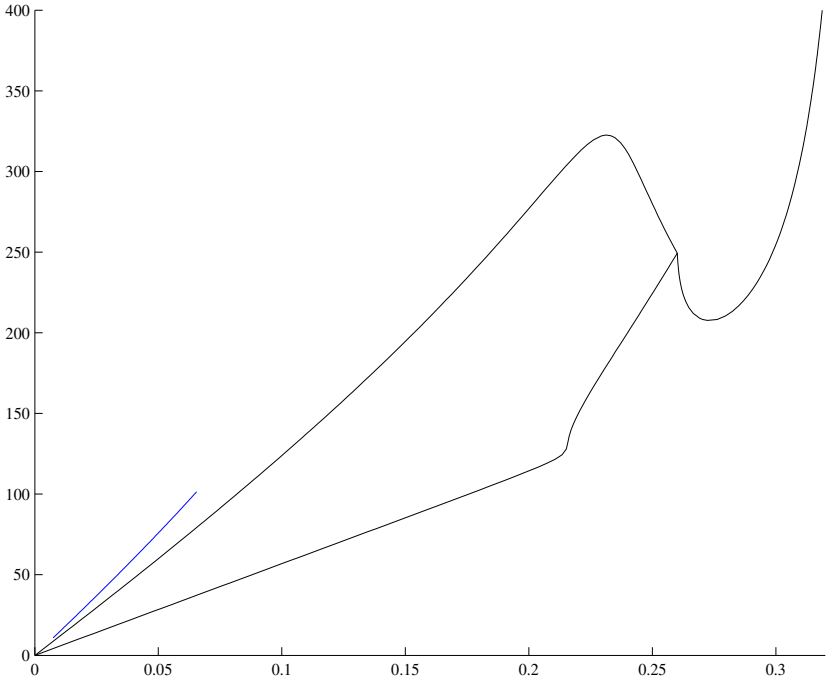


these Hopf bifurcations are subcritical. Unstable periodic orbits emanate from the Hopf bifurcations and are initially of sufficiently small amplitude to not intersect a switching manifold. However, as we move away from the Hopf bifurcations, the amplitude of the Hopf cycles grow and they graze the switching manifold along the dashed curves in Fig. 2. No bifurcation occurs at the grazing because the system is continuous [26]. As we will show in Theorem 5.4, the grazing curves intersect the Hopf loci tangentially. The unstable cycles persist beyond grazing until they collide with a stable cycle in a saddle-node bifurcation. Loci of saddle-node bifurcations of periodic orbits are not shown in the figures because we have not been able to accurately numerically compute more than a single point (when $k_La = 240$, see Fig. 2A) on the curves due to the stiffness, non-smoothness and high dimensionality of the system (2.1). We expect one such curve to emanate from (c) and lie extremely close to the upper grazing curve as has recently been shown for two-dimensional systems [27].

Fig. 2B, shows a second magnification of Fig. 1 near $D = 0.225$ and $k_La = 320$. Loci of Hopf bifurcations and saddle-node bifurcations of the equilibrium have endpoints at (d) and (e) that lie on a curve of discontinuity. We will show in Section 5 that bifurcations and dynamical behavior in neighborhoods of (d) and (e) are predicted by Theorems 5.4 and 5.1, respectively. To the left of the point (d), no bifurcation occurs along the curve of discontinuity. To the right of (e), points on the curve of discontinuity act as saddle-node bifurcations, hence we refer to these as discontinuous

local bifurcations. In Fig. 6, the period appears to go to infinity in the period-adding sequence. Within the extremely small regions

simultaneous occurrence of a saddle-node bifurcation and a discontinuous bifurcation; our results are summarized in Fig. 7A. The tangency illustrated in this figure matches our numerically computed bifurcation set, specifically point (e) of Fig. 2B. Secondly we will unfold the simultaneous occurrence of a Hopf bifurcation and a discontinuous bifurcation, see Fig. 7B. This theoretical prediction also matches numerical results, specifically the points (a), (c) and (d) of Fig. 2.

The results of this section are presented formally in Theorems 5.1 and 5.4, proofs of which are given in Appendix A. Proofs to Lemmas 5.2 and 5.3 are described in [27]. Throughout this section we use arbitrary parameters $\mu$ and $\eta$

$$\det(D_x f^{(R)}(0;0,0)) \neq 0; \tag{5.2}$$

that is, for the right-half-system, zero is not an associated eigenvalue of the origin when $\mu = \eta = 0$. Then by the implicit function theorem the right-half-system has an equilibrium, $x^{*(R)}(\mu,\eta)$, with $x^{*(R)}(0,0) = 0$ and that depends upon the parameters as a $C^k$ function in some neighborhood of the origin. As is generically the case, we may assume the distance the equilibrium is from the switching manifold varies linearly with some linear combination of the parameters. Without loss of generality we may assume $\mu$ is a suitable choice; that is

$$\frac{\partial x_1^{*(R)}(0,0)}{\partial \mu} \neq 0. \tag{5.3}$$

In this case, the implicit function theorem implies there is a $C^k$ function $\phi_1 : \mathbb{R} \to \mathbb{R}$ such that $x_1^{*(R)}(\phi_1(\eta),\eta) = 0$. In other words when $\mu = \phi(\eta)$, the equilibrium lies on the switching manifold. By performing the nonlinear change of coordinates

$$\mu \mapsto \mu - \phi_1(\eta),$$
$$x \mapsto x - x^{*(R)}(\phi_1(\eta),\eta),$$

we may factor $\mu$ out of the constant term in the system, i.e.,

$$f^{(L)}(0;\mu,\eta) = f^{(R)}(0;\mu,\eta) = \mu b(\mu,\eta) + o(k),$$

where b is $C^{k-1}$. Notice the transformation does not alter the switching manifold. The system is now

$$\dot{x} = \begin{cases} f^{(L)}(x;\mu,\eta), & x_1 \leqslant 0 \\ f^{(R)}(x;\mu,\eta), & x_1 \geqslant 0 \end{cases}, \tag{5.4}$$

with

$$f^{(i)}(x;\mu,\eta) = \mu b(\mu,\eta) + A_i(\mu,\eta)x + O(|x|^2) + o(k), \tag{5.5}$$

where $A_L$ and $A_R$ are $N \times N$ matrices that are $C^{k-1}$ functions of $\mu$ and $\eta$.

Since (5.4) is continuous, the matrices $A_L$ and $A_R$ have matching elements in all but possibly their first columns. It directly follows that the adjugate matrices (if A is non-singular, then $\operatorname{adj}(A) \equiv \det(A)A^{-1}$) of $A_L$ and $A_R$ share the same first row

Lemma 5.3. Consider the system (5.4) with (5.5) and assume that $N = 2$ and $k \geqslant 5$. Suppose $A_L(\mu, \eta)$ has complex eigenvalues $\lambda_\pm = \nu \pm i\omega$ with

(i) $\nu($

$$\{n_1, n_2, n_3\} = \left\{ e_1, \begin{bmatrix} \varphi \\ 1 \\ 0 \end{bmatrix}, e_{N+2} \right\},$$

where $n_2$ is a generalized eigenvector and $\varphi \in \mathbb{R}^N$, span $E^c$. The local center manifold, $W^c$, is tangent to $E^c$, thus on $W^c$,

$$\hat{x} = H(\hat{x}_1; \mu, \eta) = \hat{x}_1 e_1 + \mu\zeta + O(2),$$

where $\zeta \in \mathbb{R}^N$ is equal to $\varphi$ except that its first element is zero. Notice $\xi^T(0,0)V = e_1^T$ thus

$$\hat{x}_1 = e_1^T \hat{x} = \xi^T(0,0)V\hat{x} = \xi^T(0,0)x.$$

Restricted to $W^c$ the dynamics (A.2) become the $C^{k-1}$ system

$$\begin{aligned} \dot{\hat{x}}_1 = {} & \mu\xi^T(0,0)b(\mu,\eta) + \xi^T(0,0)A_L(\mu,\eta)VH(\hat{x}_1;\mu,\eta) \\ & + \xi^T(0,0)g^L(VH(\hat{x}_1;\mu,\eta);\mu,\eta), \end{aligned} \tag{A.4}$$

where $g^L(\hat{x};\mu,\eta)$ denotes the terms of the Taylor series of $f^L(x;\mu,\eta)$ near $x = 0$. By expanding each term in